Letters

A Bidirectional Wireless Power Transfer EV Charger Using Self-Resonant PWM

Jun-Young Lee and Byung-Moon Han

***Abstract*—This letter suggests a large air-gap bidirectional wireless power transfer charger for electric vehicle. It is controlled by pulse width modulation with a self-resonant frequency formed by self-inductance and resonant capacitor so that constant frequency operation can be accomplished under large air-gap without additional current chopper. The feasibility of the proposed method has been verified with a 6.6-kW prototype with air-gap of 12–20 cm.**

***Index Terms*—Battery charger, bidirectional converter, wireless power transfer (WPT).**

I. Introduction

ELECTRIC vehicle (EV) provides an opportunity to employ vehicle-to-grid technology to make it an energy storage device by providing the battery power to the grid or the local loads [1]–[3]. Recently, WPT in EV has been studied by many researchers due to advantages such as convenience of wireless charging and safety in high-power transfer [4], [5]. Wireless power transfer (WPT) systems for EV must have high efficiency, a large air-gap, and good tolerance for misalignment. To meet these requirements, several papers have suggested solutions such as current chopping method [6], [7] and variable frequency control method [8], [9]. The current chopping method has a two-stage structure comprised of WPT stage with constant or variable switching frequency and pulse width modulation (PWM) chopper stage for load regulation. However, it suffers from low system efficiency due to low chopper efficiency and irregular pulse skipping, and it is applicable only for unidirectional applications. The variable frequency control method has a single-stage structure, but it cannot be used for applications that require a fixed frequency.

In this letter, an alternative approach for a large air-gap bidirectional WPT EV charger is suggested. It is controlled by self-resonant PWM (SR-PWM) operated with a frequency formed by self-inductance and resonant capacitor. The proposed method provides constant frequency operation regardless of air-gap and does not require additional current chopper. Also it has more high gain as air-gap is increased, which facilitates power transfer under wide air-gap.

Manuscript received May 6, 2014; revised July 2, 2014; accepted July 28, 2014. Date of current version November 3, 2014. This work was supported by the Human Resources Development Program (No. 20114010203030) of the Korea Institute of Energy Technology Evaluation and Planning (KETEP), and Grant funded by the Korea Government Ministry of Trade, Industry, and Energy. Recommended for publication by Associate Editor H. Chung.

The authors are with the Department of Electronics Engineering, Myongji University, Yongin-Si 449-728, Korea (e-mail: pdpljy@mju.ac.kr; erichan@mju.ac.kr).

Digital Object Identifier 10.1109/TPEL.2014.2346255

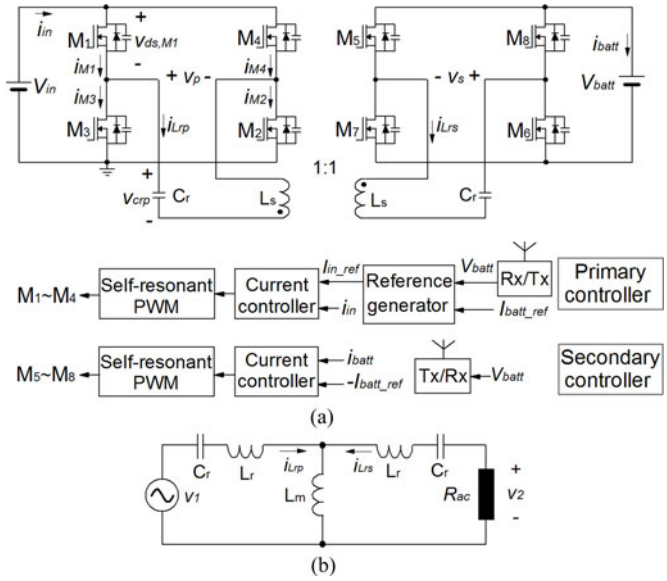

Fig. 1. (a) Proposed WPT charger and (b) its ac-equivalent circuit.

II. Proposed WPT Charger

A. Description of the Proposed Method

Fig. 1(a) shows the proposed SR-PWM wireless charger. Primary and secondary coils are coupled through air with the gap of several tens of centimeters. Primary and secondary controllers deal with charging and discharging modes respectively. In charging mode, primary switches are used for charging control through a primary controller. However, since charging current is located on the secondary side, it is not easy to control charging current directly due to a large wireless communication delay time with over several tens of milliseconds. To overcome this problem, the primary controller deals with the charging current indirectly through input current that is calculated using battery voltage. If structures of two coils are same and turns ratio is unity, leakage inductances in primary and secondary coils can have a same value of L_r. Also, since primary self-inductance L_s is equal to sum of L_r and the magnetizing inductance referred to the primary side L_m, the equivalent circuit of coils and ac-equivalent circuit of proposed wireless charger in CM can be depicted in Fig. 1(b). v_1 and v_2 are the fundamental harmonics of v_p and v_s, respectively, and R_{ac} is the ac-equivalent load

resistor [10]. Their frequency-domain expressions according to angular switching frequency ω_s are

$$R_{\rm ac} = 8V_{\rm batt}/(\pi^2 I_{\rm batt}) \quad (1)$$

$$V_1(j\omega_s) = [(4V_{\rm in}/\pi)\sin D\pi]\angle 0^\circ \quad (2)$$

$$V_2(j\omega_s) = (4V_{\rm batt}/\pi)\angle\theta^\circ \quad (3)$$

where D is the duty ratio, and θ is the phase angle between $\rm v_1$ and $\rm v_2$. From an ac-equivalent circuit, the transconductance gain defined by $G_{ip}(\rm j\omega_s) = I_{Lrp}(\rm j\omega_s)/V_1(\rm j\omega_s)$ can be derived as, (4) as shown at the bottom of the page.

With (4), $V_2(\rm j\omega_s)$, and $I_{Lrs}(\rm j\omega_s)$ can be written as follows:

$$V_2(j\omega_s) = G_{ip}(j\omega_s)\frac{-\omega_s^2 L_m C_r R_{\rm ac}}{(1-\omega_s^2 L_s C_r)+j\omega_s C_r R_{\rm ac}} \times V_1(j\omega_s) \quad (5)$$

$$I_{Lrs}(j\omega_s) = G_{ip}(j\omega_s)\frac{\omega_s^2 L_m C_r}{(1-\omega_s^2 L_s C_r)+j\omega_s C_r R_{\rm ac}} \times V_1(j\omega_s). \quad (6)$$

At the self-resonant frequency $\omega_{\rm Ls} = 1/(C_r L_s)^{0.5}$, (4), (5), and (6) are rewritten as follows:

$$I_{Lrp}(j\omega_{Ls}) = [R_{\rm ac}/(\omega_{Ls}^2 L_m^2)] \times V_1(j\omega_s) \quad (7)$$

$$V_2(j\omega_{Ls}) = [-R_{\rm ac}/(j\omega_{Ls} L_m)] \times V_1(j\omega_s) \quad (8)$$

$$I_{Lrs}(j\omega_{Ls}) = [1/(j\omega_{Ls} L_m)] \times V_1(j\omega_s). \quad (9)$$

The peak value of the primary resonant current I_{Lrp}, pk at ω_{Ls} can be derived as

$$I_{\rm Lrp,pk} = 4V_{\rm batt}/(\pi\omega_{Ls} L_m) \quad (10)$$

from (2), (3), (7), and (8). Referring to (7), (9), and (10), the primary resonant current has same phase angle with the fundamental harmonic of v_p and its peak value is constant according to battery voltage and magnetizing inductance. Also, primary resonant current i_{Lrp} leads the secondary resonant current $\rm i_{Lrs}$ by 90°. Since the charging current $\rm I_{batt}$ is equal to the mean value of $\rm i_{Lrs}$, $\rm I_{batt}$ can be expressed as

$$I_{\rm batt} = 8V_{\rm in}\sin D\pi/(\pi^2\omega_{Ls} L_m) \quad (11)$$

from (2) and (9). $\rm I_{batt}$ in discharging mode can be derived from same procedure with charging mode, and it can be written as follows:

$$I_{\rm batt} = -8V_{\rm batt}\sin D\pi/(\pi^2\omega_{Ls} L_m). \quad (12)$$

It shows that the battery current can be controlled with simple PWM control. Also, as magnetizing inductance decreases, the operational duty ratio also decreases.

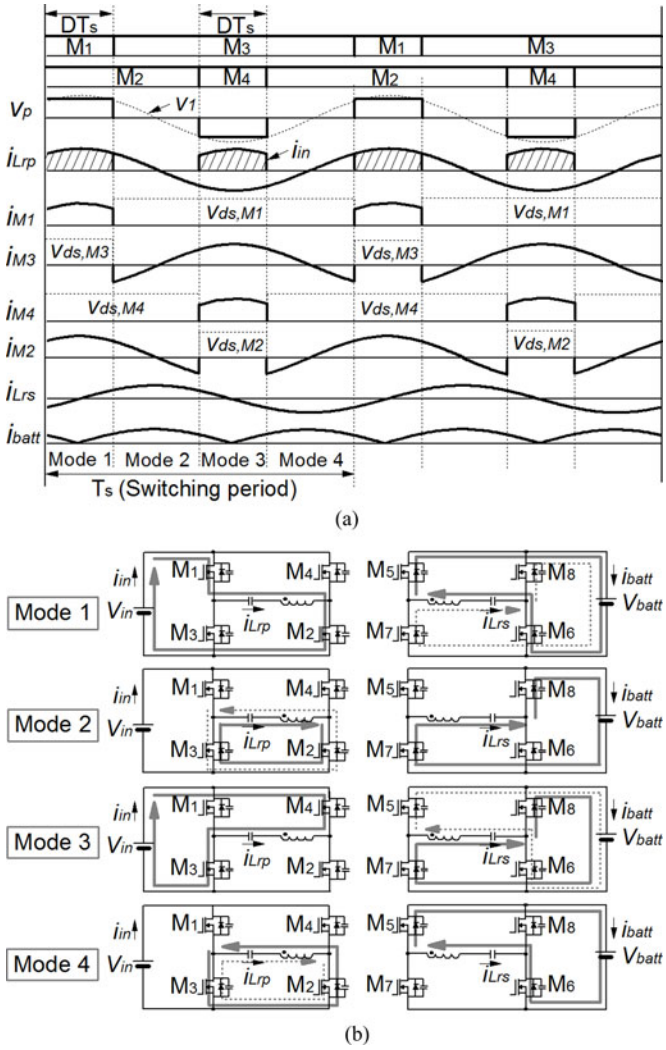

Fig. 2. Operational waveforms and mode diagrams.

B. Operational Mode Analysis

Because charging and discharging operations are same, operational modes are explained only with charging operation. Before analysis, it is assumed that PWM frequency is same with self-resonant frequency. The operational waveform of the proposed method can be depicted in Fig. 2. Since $\rm i_{Lrp}$ is constant in case that battery voltage and the air-gap are fixed, the current control can be accomplished only by changing duty ratio of $\rm M_1$ and $\rm M_4$. When $\rm M_1$ is turned ON, mode 1 begins. During mode 1, $\rm i_{Lrp}$ flows through $\rm M_1$, C_r, primary coil, and $\rm M_2$. Since $\rm i_{Lrs}$ lags $\rm i_{Lrp}$ by 90°, the path of $\rm i_{Lrs}$ is changed from body diodes of $\rm M_5$ and $\rm M_6$ to body diodes of $\rm M_7$ and $\rm M_8$. After $\rm M_1$ is turned OFF and $\rm M_3$ is turned ON, $\rm i_{Lrp}$ circulates through $\rm M_3$ and $\rm M_2$. During mode 2, $\rm i_{Lrs}$ is still positive current so that conduction path is formed with body diodes of $\rm M_7$ and $\rm M_8$. Operations of modes

$$G_{ip}(j\omega_s) = \frac{\omega_s C_r(1-\omega_s^2 C_r L_s) + j\omega_s^2 C_r^2 R_{\rm ac}}{\omega_s C_r(1-\omega_s^2 C_r L_s)R_{\rm ac} + j(1-\omega_s^2 L_r C_r)(\omega_s^2 L_r C_r + 2\omega_s^2 L_m C_r - 1)} \quad (4)$$

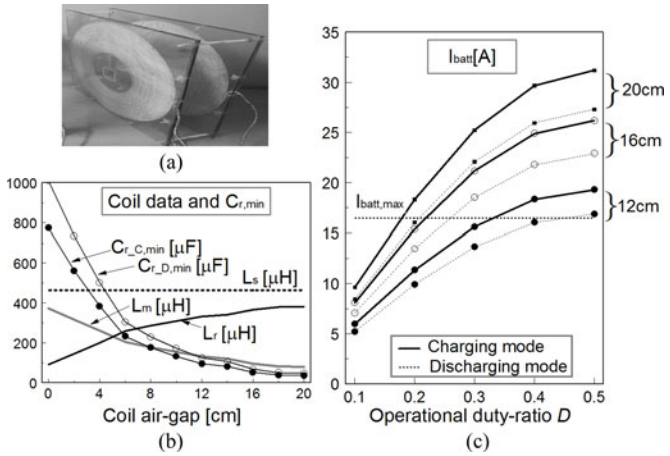

Fig. 3. (a) Implemented coil, (b) measured inductance data and minimum C_r's according to air-gap, and (c) controllable battery current according to duty ratio and air-gap.

3 and 4 are similar to those of modes 1 and 2. As shown in operational waveforms in Fig. 2, switch currents of M_2 and M_3 are negative at switching instants so that there are no switching losses in these two switches.

C. Design Guidelines

Referring to operational waveform in Fig. 2, D should be smaller than 0.5. Based on this condition and (11) and (12), the resonant capacitor can be designed with the following inequality:

$$\text{Charging mode: } C_{r\_C} \geq \left(\pi^2 I_{\text{batt}} L_m / 8 V_{\text{in}}\right)^2 / L_s \qquad (13)$$

$$\text{Discharging mode: } C_{r\_D} \geq \left(\pi^2 I_{\text{batt}} L_m / 8 V_{\text{batt}}\right)^2 / L_s. \qquad (14)$$

To guarantee the bidirectional operation, C_r should be designed to meet these two inequalities.

III. Experimental Results

The prototype has been designed with 6.6 kW ($V_{\text{in}} = 400$ V, $V_{\text{batt}} = 350\,\text{V} \sim 450\,\text{V}/I_{\text{batt.max}} = 16.5$ A, air-gap $= 12$ cm $\sim$20 cm). The selected switching devices are M_1–M_4 = IPW65R041CFD $\times$ 2 and D_1–D_4 = FFH60UP40S. The controller has been implemented with TMS320F28335 and Bluetooth was used to transfer the battery voltage through wireless communication. Fig. 3(a) shows the implemented coil. Both of primary and secondary coils have a circular-pad type structure (coil diameter = 50 cm) implemented with 35 turns (Litz wire of 0.12 mm/600strands) and air core. Each coil resistance is 0.14 Ω and measured inductance data according to air-gap is as shown in Fig. 3(b). Based on the coil data and design specifications, the minimum C_r according to air-gap is superimposed on this graph. The minimum C_r at air-gap = 12 cm is calculated as 126 nF and we have used 132 nF considering duty-ratio margin. The self-resonant frequency becomes 20.3 kHz and the charger is also operated with this frequency. The charging current according to duty ratio changes, depicted in Fig. 3(c), shows that the prototype satisfies the maximum charging current under bidirectional operation and power transfer is more easier under wide air-gap. Fig. 4 is the measured waveforms under various conditions and efficiency plot at $V_{\text{batt}} = 400$ V. It shows that the primary resonant current has same waveform regardless of load conditions as explained in Section II. Also, the resonant frequency is not affected by air-gap changes and the proposed method is well operated under coil misalignment. The measured

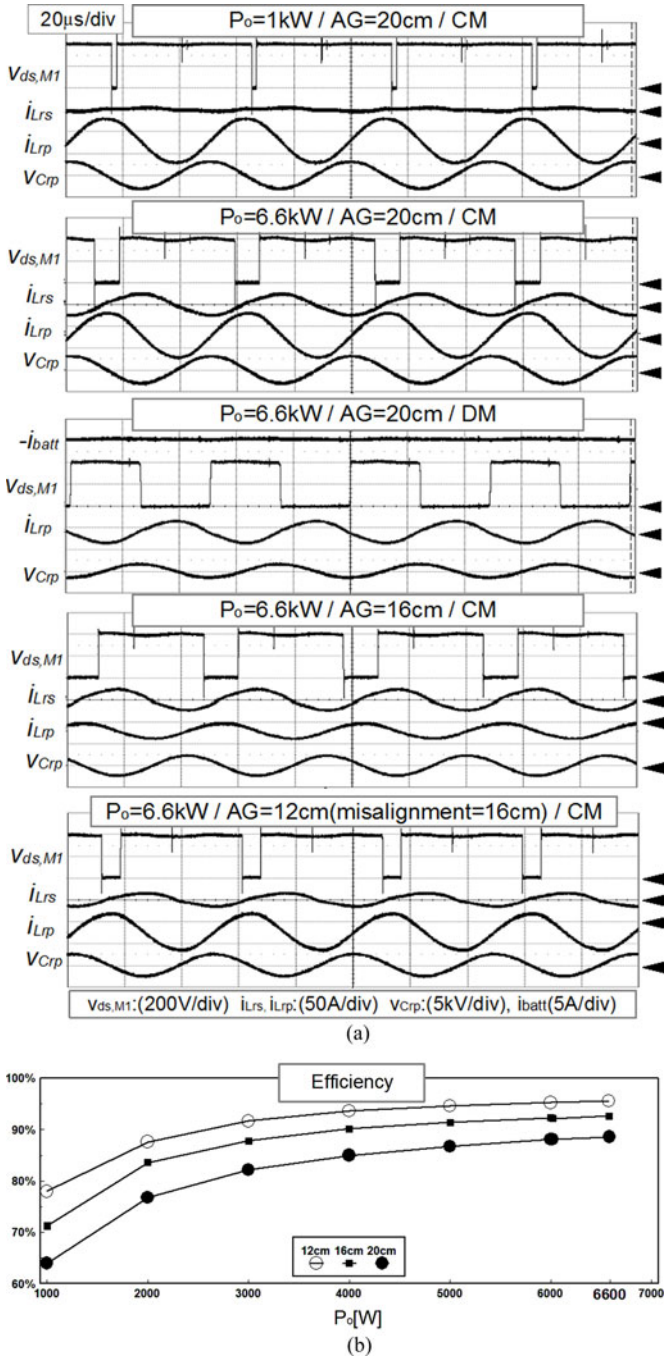

Fig. 4. Measured waveforms under various conditions and (b) efficiency plot at $V_{\text{batt}} = 400$ V (AG: air-gap, CM: charging mode, DM: discharging mode).

efficiencies according to air-gap are in the range of 88.1–95.3% at full-load condition.

IV. Conclusion

In this letter, a large air-gap bidirectional WPT EV charger with SR-PWM method has been proposed. The proposed method has a simple structure without additional current chopper and it can cope with a large air-gap power transfer with constant frequency PWM. Operation has been analyzed and design guideline has been derived based on this analysis. To verify the performance, a 6.6-kW prototype charger with air-gap of 12–20 cm has been implemented with the design guideline and efficiency of 88.1–95.3% has been recorded at full load condition. Therefore, it may be suitable for bidirectional wireless chargers requiring for large air-gap and constant switching frequency.

References

[1] L. Jian, H. Xue, G. Xu, X. Zhu, D. Zhao, and Z. Y. Shao, "Regulated charging of plug-in hybrid electric vehicles for minimizing load variance in household smart microgrid," *IEEE Trans. Ind. Electron.*, vol. 60, no. 8, pp. 3128–3226, Aug. 2013.

[2] T. S. Ustan, A. Zayegh, and C. Ozansoy, "Electric vehicle potential in Australia: Its impact on smartgrids," *IEEE Ind. Electron. Mag.*, vol. 60, no. 4, pp. 15–25, Dec. 2013.

[3] S. Shopra and P. Bauer, "Driving range extension of EV with on-road contactless power transfer-a case study," *IEEE Trans. Ind. Electron.*, vol. 60, no. 1, pp. 329–338, Jan. 2013.

[4] H. Takanashi, Y. Sato, Y. Kaneko, S. Abe, and T. Yasuda, "A large air gap 3 kW wireless power transfer system for electric vehicles," in *Proc. Energy Convers. Congr. Expo.,* 2012, pp. 269–274.

[5] F. Musavi, M. Edington, and W. Eberle, "Wireless power transfer: A survey of EV battery charging technologies," in *Proc. Energy Convers. Congr. Expo.,* 2012, pp. 1804–1801.

[6] M. A. Bloom, N. Geng, and M. Krishnamurthy, "Design considerations for wireless electric vehicle charging," in *Proc. Transp. Electr. Conf. Expo.,* 2013, pp. 1–6.

[7] H. H. Wu, A. Gilchrist, K. D. Sealy, and D. Bronson, "A high efficiency 5 kW inductive charger for EVs using dual side control," *IEEE Trans. Ind. Informat.*, vol. 8, no. 3, pp. 585–595, Jan. 2012.

[8] R. M. Miskiewicz, A. J. Moradewicz, and M. P. Kazmierkowski, "Contactless battery charger with bi-directional energy transfer for plug-in vehicles with vehicle-to-grid capability," in *Proc. IEEE Int. Symp. Ind. Electron.,* 2011, pp. 1969–1973.

[9] U. K. Madawala, M. Neath, and D. J. Thrimawithana, "A power–frequency controller for bidirectional inductive power transfer systems," *IEEE Trans. Ind. Electron.*, vol. 60, no. 1, pp. 310–317, Jan. 2013.

[10] R. Beiranvand, M. R. Zolghadri, B. Rashidian, and S. M. H. Alavi, "Optimizing the LLC–LC resonant converter topology for wide-output-voltage and wide-output-load applications," *IEEE Power Electron.*, vol. 26, no. 11, pp. 3192–3204, Nov. 2011.